Chapter 5

Isomorphous Substitution in Bimetallic Oxide Clusters

5.1 Introduction

The size- and composition-dependent properties of gas phase transition metal oxide clusters have intensely been studied to gain a better understanding of the elementary steps in heterogeneous catalysis [185]. A long sought-after goal, in this regard, has been the tailoring of the electronic and geometric structure of clusters by carefully choosing the cluster composition. However, this approach has been limited up to now by the availability of adequate cluster sources. Specifically, it is clear that, while changing the size and composition of clusters, *both* the geometric and the electronic structures are in general modified. It is therefore difficult to understand what is the specific promoter of an observed property.

The goal of the present study is to make use of mixed metal oxides to modify the electronic and the geometric configuration of clusters, independently of each other. In particular, one or more vanadium atoms (group +V) are replaced by titanium atoms (group +IV) in the metal oxide cluster, in order to change the number of valence electrons, but keeping the metal atom radius roughly constant.

This kind of substitution had already been successfully applied to pure metal clusters, but never for metal oxides. For pure metal clusters, physical systems composed of a limited number of fermions, such as atoms and atomic nuclei, some basic properties are described by simple shell models, which have been successfully adopted to explain size-dependent properties of metal nanoclusters and semiconductors quantum dots [1, 186–188]. Particularly important for all these few-fermion systems is their shape and symmetry. The investigation of bimetallic clusters allows to tune the number of fermions (the number of delocalized electrons governs the shell model interpretation) and the confining potential (formed by the ion cores) independently (see

Janssens et al. [189] and references therein). In the last years, Lievens and coworkers have performed pioneering photofragmentation experiments focused on mixed metal clusters of coinage metals doped with one or a few transition metal atoms [189–191]. Their investigations focused on the influence of the dopant atom on the electronic shell structure and the geometry of the clusters. They investigated the interplay between free electrons (coinage metals) and more directional bonds (transition metals) and found that introducing a dopant atom in a metal cluster can change its structure and electronic properties unexpectedly [190–192].

In the present study on mixed vanadium-titanium oxide clusters, it is shown that it is indeed possible to modify the electronic configuration of a cluster without transforming the overall geometry. The results presented here are the first IR spectra of mixed metal oxides. The systems chosen for these first experiments are the $(V_2O_5)_n^-$ clusters (n=2–4) studied in Chapter 3. These clusters form polyhedral cages made of $(-O)_3V{=}O$ units. Opposite to the neutral $(V_2O_5)_n$ cages [111], the anionic clusters are open shell systems; they have one unpaired electron in vanadium d states. While the unpaired electron is fully delocalized over all vanadium atoms in n=2, it localizes on a single atom for the larger clusters [104]. With the experiments presented in this chapter, this study is extended in two series of experiments. First, a single vanadium atom is replaced by a titanium atom, yielding closed-shell $(V_2O_5)_{n-1}(VTiO_5)^-$ anions isoelectronic with the neutral $(V_2O_5)_n$ clusters. Second, the number of atoms is kept constant, but each vanadium atom in $V_4O_{10}^-$ is sequentially exchanged by a titanium atom corresponding to an oxidation of the cluster.

5.2 Experimental Details

Vanadium oxide, titanium oxide, and mixed vanadium-titanium oxide cluster anions are produced with a dual target laser vaporization source (see Section 2.1). The source runs at 10 Hz. The helium carrier gas contains 1% of oxygen, yielding oxygen saturated cluster growth conditions. For every species overview spectra are at first recorded with low resolution at 0.1 μm step size, to identify the absorption bands. Every peak is then scanned with higher resolution (in 0.01 μm steps), and the necessary laser attenuation to avoid saturation of the spectra. FELIX is coupled to the tandem mass spectrometer using the KRS-5 setup (see Section 2.2).

5.3 Results and Discussion

5.3.1 Mass Spectra

The mass spectra of bimetallic oxides are more complex than for monometallic oxide clusters. At first, mass spectra of vanadium oxide anions, titanium oxide anions and

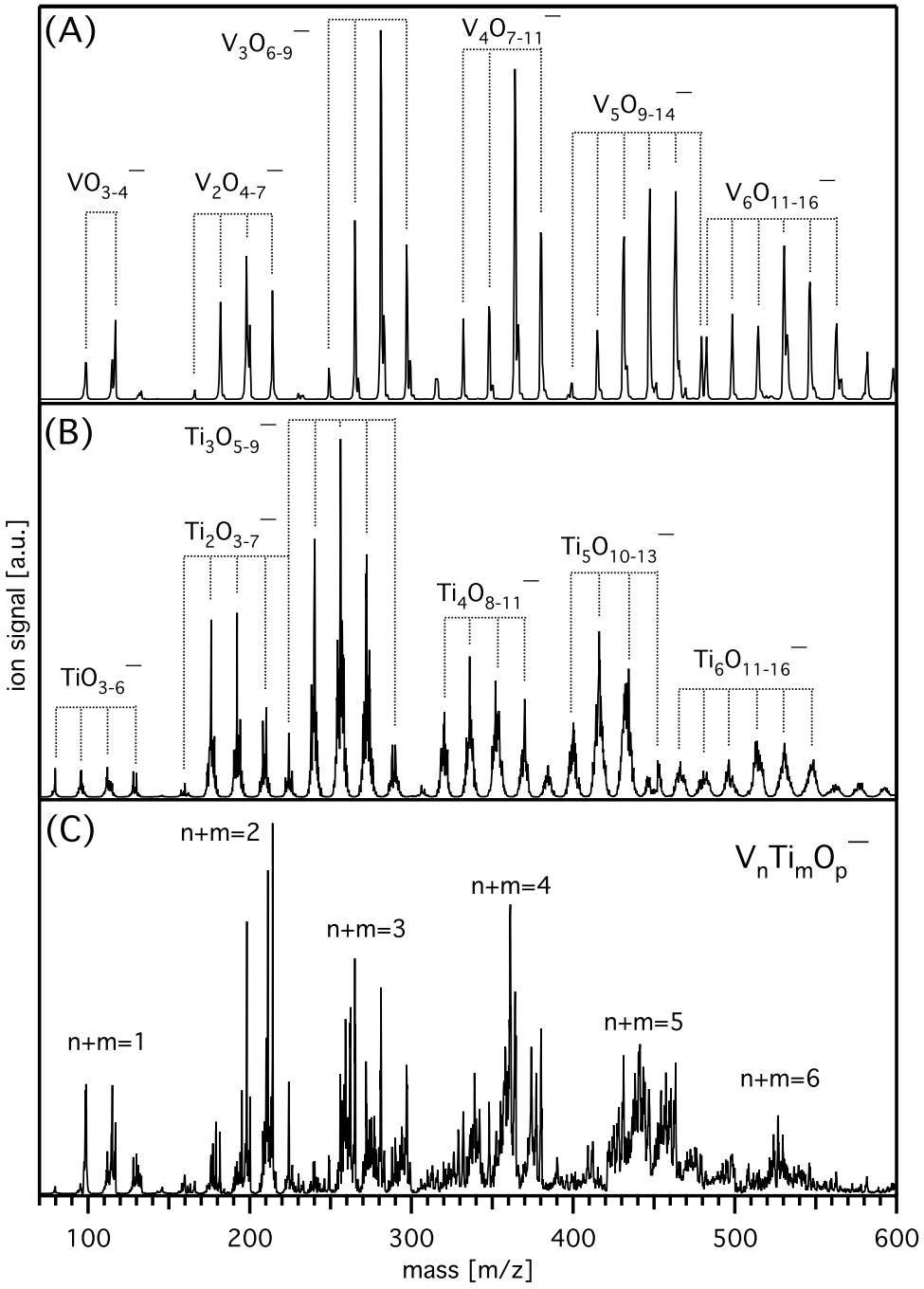

Figure 5.1: Mass spectra of (A) vanadium oxide, (B) titanium oxide, and (C) mixed vanadium titanium oxide cluster anions. 1% oxygen concentration in helium carrier gas is used. All source parameters are similar for the three spectra.

mixed vanadium-titanium oxides anions, produced under similar conditions are compared. In particular, the same oxygen concentration, the same gas backing pressure, gas pulse duration, and laser-gas pulse delay are used. Laser powers for the two different metals cannot be exactly the same, given the different reflectivity of the surfaces and the different evaporation energies. In Figure 5.1 (A) a typical mass spectrum of vanadium oxide anions is shown, $V_nO_p^-$, for n=1–8. The peaks are organized in groups centered on the $p/n = 2.5$ vanadium to oxygen stoichiometric ratio. These groups are well separated for $n \leq 4$. For larger n's the groups partially overlap. For example, $V_6O_{15}^-$ (546 amu), $n = 6$ group, is represented by a signal of $5.5{\cdot}10^4$ counts/s; whereby $V_7O_{12}^-$ (549 amu), the closest peak from the neighboring group $n = 7$, has a signal of $5{\cdot}10^3$ counts/s—more than ten times lower. $V_8O_9^-$ (552 amu), the closest peak from the second next group $n = 8$, has a signal of about 10 counts/s, which is within the noise level. However, this partial overlap of the groups with different n in the mass spectrum is not of any concern in the case of pure vanadium oxide anions, because the unitary mass resolution of the quadrupoles is capable of separating the cluster of interest.

In Figure 5.1 (B) a typical mass spectrum of titanium oxide anions is shown, $Ti_mO_p^-$, for m=1–6. The peaks are organized in groups centered on the $p/m \simeq 2.3$ vanadium to oxygen stoichiometric ratio. The mass peaks are broader than in the vanadium oxide anions mass spectrum due to the isotope distribution of titanium. The abundance of the titanium isotopes relative to the 48 amu isotope (100%) are 11.2% for mass 46, 10.1% for mass 47, 7.3% for mass 49, and 7.0% for mass 50. Note that the mass of the most abundant titanium isotope, ^{48}Ti, equals three times the mass of oxygen (16 amu). As in the case of vanadium oxides, the overlap between groups of peaks belonging to different m values is only partial. The overall distributions of $V_nO_p^-$ and $Ti_mO_p^-$ are similar to those observed before [97, 104, 117, 193]. Investigations on neutral clusters using post-ionization, however, give a lower oxygen to metal ratio [173, 194], most probably because of the higher ionization potential of highly oxidized clusters [117]. The mass spectrum of the bimetallic oxide clusters is considerably more complex, since many (n, m, p) combinations are possible for the same mass (see Figure 5.1 (C)). To investigate the singly titanium doped clusters ($V_3TiO_{10}^-$, $V_5TiO_{15}^-$, and $V_7TiO_{20}^-$), the titanium content in the cluster beam is kept low not to create a lot of titanium-rich species. This simplifies the analysis of the mass spectra. The masses of the singly titanium doped species are 3 amu lower than the corresponding vanadium oxide clusters ($V_4O_{10}^-$, $V_6O_{15}^-$, and $V_9O_{20}^-$). This difference can easily be resolved by the mass filters. However, to investigate the titanium-rich clusters the titanium content in the cluster beam needed to be increased. For these clusters ($V_2Ti_2O_{10}^-$, $VTi_3O_{10}^-$, and $Ti_4O_{10}^-$) a complete mass separation is not possible because different clusters can have the same mass due to the titanium isotope distribution. The $V_{4-n}Ti_nO_{10}^-$ (n=0–4) IR-PD spectra are measured after mass selection of the 352, 355, 358, and 361 amu signals (marked with asterisks in Figure 5.2),

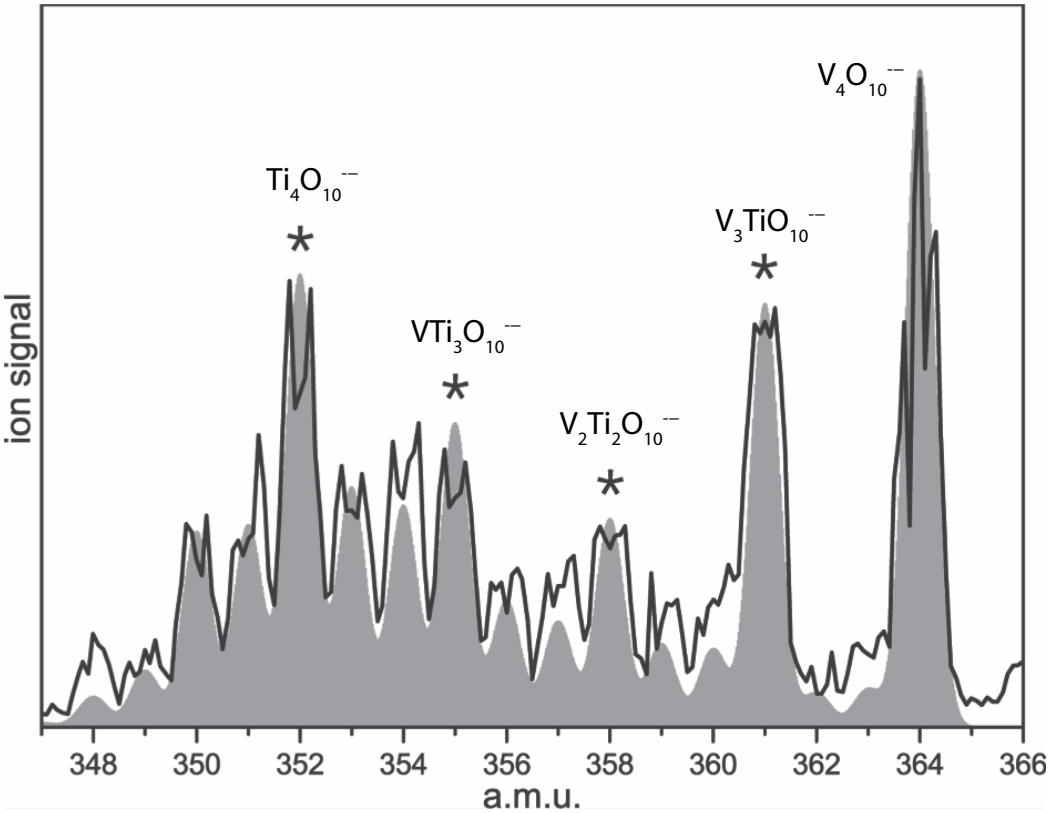

Figure 5.2: Experimental mass spectrum of mixed vanadium-titanium oxide cluster anions, $V_{4-n}Ti_nO_{10}^-$ (n=0–4), compared with a mass distribution calculated on the basis of the natural isotope patterns. Cluster for which IR-PD spectra are measured are marked with asterisks. For contamination rates, see Table 5.1

	$V_3TiO_{10}^-$	$V_2Ti_2O_{10}^-$	$VTi_3O_{10}^-$	$Ti_4O_{10}^-$
contaminant				
$V_2Ti_2O_{10}^-$	0.7%	—	1%	—
$VTi_3O_{10}^-$	—	5%	—	5%
$Ti_4O_{10}^-$	—	—	10%	—
total	0.7%	5%	11%	5%

Table 5.1: Contamination of $V_{4-n}Ti_nO_{10}^-$ (n=1–4) clusters. Results from the fitting of a calculated mass distribution on the basis of natural isotope abundance to the experimental mass spectrum.

which correspond to the mass of the most abundant titanium isotopomer—the pure $V_4O_{10}^-$ cluster is not discussed in this Section, since it does not present this kind of difficulties. To check for an overlap of different cluster compositions at the selected masses, the measured mass spectrum is compared in the 346–366 amu region with a $V_{4-n}Ti_nO_{10}^-$ (n=0–4) distribution, taking into account the natural isotope patterns (see Figure 5.2). All peaks are convoluted with a Gaussian line shape of 0.5 amu FWHM. From the calculated distribution one obtains the contamination ratios reported in Table 5.1. Given the good agreement between calculated distribution and measured mass spectrum contamination rates appear to be estimated correctly. The most contaminated cluster (11% contamination) is $VTi_3O_{10}^-$, which might lead to additional minor peaks in the IR-PD spectrum.

5.3.2 IR Spectra

IR-PD spectra are measured for two cluster series. First, the influence of substituting a single vanadium atom by a titanium atom for $(V_2O_5)_{n-1}(VTiO_5)^-$ (n=2–4) is studied. Then the effect of the sequential replacement of V by Ti in $V_{4-n}Ti_nO_{10}^-$ (n=0–4) clusters is examined. The observed fragmentation channels are listed in Table 5.2. Note that different clusters can yield the same fragment, implying that double mass selection is imperative for these measurements. IR-PD spectra of singly substituted vanadium oxide anions are shown in the top panel of Figure 5.3. The spectra are obtained by monitoring the fragment ion denoted with asterisks in Table 5.2 in dependence on FELIX photon energy.

The dissociation upon IR irradiation of $V_3TiO_{10}^-$, $V_5TiO_{15}^-$, and $V_7TiO_{20}^-$ is governed by the formation of two closed-shell fragments. All three species form $V_3O_8^-$, but the most abundant fragment for the two larger anions is $V_3TiO_{10}^-$. The IR-PD spectra of the $(V_2O_5)_{n-1}(VTiO_5)^-$ (n=2–4) series are characterized by three absorption regions: (*i*) a sharp peak around 1000 cm^{-1}, (*ii*) a broad and intense band in the 800–950 cm^{-1} region, and (*iii*) a weaker absorption band around 700 cm^{-1} (see Table 5.3)

To assist the structural assignment, DFT geometry optimization are carried out in the Sauer group (Humboldt-Universität zu Berlin, Germany). Their DFT calculations are done using the TURBOMOLE program [118], employing the B3LYP hybrid functional [119] and the TZVP basis sets [120]. Harmonic frequencies are scaled using a 0.9429 multiplicative factor [113]. The calculated spectra are convoluted with a Gaussian line shape of 20 cm^{-1} FWHM for better comparison with the experimental spectra (bottom panel of Figure 5.3).

Polyhedral cage structures in which each metal atom M forms a terminal M=O double bond and takes part in three M−O−M single bond bridges, are found as lowest energy isomers for the closed-shell $(V_2O_5)_{n-1}(VTiO_5)^-$ (n=2–4) clusters. Their simulated infrared absorption spectra agree satisfactorily with the experimental IR-

Cluster	Fragment ion	Relative abundance (%)	Lost neutral
$V_7TiO_{20}^-$	$*V_3TiO_{10}^-$	100	V_4O_{10}
	$V_3O_8^-$	64	V_4TiO_{12}
$V_5TiO_{15}^-$	$*V_3TiO_{10}^-$	100	V_2O_5
	$V_3O_8^-$	64	V_2TiO_7
$V_3TiO_{10}^-$	$V_3TiO_9^-$	26	O
	$*V_3O_8^-$	100	TiO_2
	$V_3O_7^-$	24	TiO_3
	$V_2TiO_7^-$	33	VO_3
	VO_3^-	12	V_2TiO_7
$V_2Ti_2O_{10}^-$	$V_2Ti_2O_9^-$	38	O
	$*VTi_2O_7^-$	100	VO_3
$VTi_3O_{10}^-$	$VTi_3O_9^-$	100	O
	$*VTi_2O_7^-$	46	TiO_3
	$Ti_3O_7^-$	12	VO_3
$Ti_4O_{10}^-$	$Ti_4O_9^-$	96	O
	$Ti_4O_8^-$	100	O_2
	$*Ti_3O_7^-$	54	TiO_3
$V_4O_{10}^-$	$*V_3O_8^-$	100	VO_2

Table 5.2: Relative abundances of the IR fragmentation channels of $V_nTi_mO_p^-$. Fragments monitored in the IR-PD study are marked with asterisks. Fragments with relative abundances lower than 10% are not listed.

PD spectra (Figure 5.3), yielding the following assignment for the three absorption regions. The narrow bands at 976, 1001, and 1005 cm^{-1} for the n=2–4 are due to the $2n-1$ V=O and to the $Ti^{(-)}$=O stretching mode, in good agreement with the 975 cm^{-1} stretching mode of compounds with titanyl groups in solution [195] and with stretches of vanadyl groups in anionic $(V_2O_5)_n^-$ [104] and neutral $(V_2O_5)_n$ (see Figure 5.6) clusters. The broad bands with maxima at 821 cm^{-1} ($V_3TiO_{10}^-$), 883 cm^{-1} ($V_5TiO_{15}^-$), and 885 cm^{-1} ($V_7TiO_{20}^-$) are assigned to the symmetric and antisymmetric stretches of the $M-O-M$ bridges. The width of this band is considerably broader in the experimental spectra than in the calculated ones (similarly to the IR-PD spectra of the larger vanadium oxide anions in Chapter 3, see also Ref. [104]) and is tentatively attributed to pronounced inter-mode coupling, which is completely neglected within the harmonic approximation and therefore not well reproduced in the simulated spectra. Finally, the absorption below 800 cm^{-1} is due to vibrational modes involving larger parts of the cluster. In Figure 5.4 the calculated structures for vanadium oxide and singly substituted cluster anions are shown. Although the sym-

Parent	Fragment	Position of Observed Bands (cm^{-1})
$V_3TiO_{10}^-$	$V_3O_8^-$	976, 821, 815(s), 810(s), 693, 628, 610
$V_5TiO_{15}^-$	$V_3TiO_{10}^-$	1001, 989(s), 955, 883, 865, 859(s), 712(s), 700, 695
$V_7TiO_{20}^-$	$V_3TiO_{10}^-$	1007, 965, 916, 904(s), 887, 820(s), 787 764, 708, 694(s)

Table 5.3: Experimental vibrational frequencies (in cm^{-1}) of $(V_2O_5)_{n-1}(VTiO_5)^-$ (n=2–4) cluster anions determined from the respective IR-PD spectra, measured monitoring fragment ions mass-selectively. Vibrational frequencies are determined from band maxima or estimated based on observable shoulders (s) formed by overlapping transitions.

metries are lowered by the presence of the titanium atom, the geometric structures remain the same.

The IR-PD spectra for the $V_{4-n}Ti_nO_{10}^-$ (n=0–4) clusters are shown in the top panel of Figure 5.5. Both $V_4O_{10}^-$ and $V_3TiO_{10}^-$ fragment to $V_3O_8^-$ upon irradiation with resonant IR photons (see Table 5.2 and Chapter 3). The main fragmentation channel of $V_2Ti_2O_{10}^-$ is the formation of $VTi_2O_7^-$. $VTi_3O_{10}^-$ and $Ti_4O_{10}^-$ are oxygen richer and consequently the loss of molecular (for $Ti_4O_{10}^-$) of atomic oxygen is prominent (see Table 5.2). These observations are in line with collision induced dissociation experiments on vanadium oxide clusters with a high oxygen to metal ratio for which loss of weakly bound O_2 and O species was reported [97].

All IR-PD spectra of $V_{4-n}Ti_nO_{10}^-$ (n=0–4) have a sharp band slightly below 1000 cm^{-1}. Except for $V_4O_{10}^-$, all spectra have a broad and intense band around 780–850 cm^{-1}. For n=2–4, the vibrational structures below 750 cm^{-1} are richer than for the pure $V_4O_{10}^-$ and closed-shell $V_3TiO_{10}^-$. All absorption bands for these cluster anions are summarized in Table 5.4.

On the basis of the DFT calculations, structures for n=0–3 clusters can be assigned. In Figure 5.5 experiments and calculations are compared. The most stable structures found computationally for $V_{4-n}Ti_nO_{10}^-$ (n=0–3) all have a tetrahedral shape similar to the geometry of $V_4O_{10}^-$. Electronically the clusters with n=2 and 3 are in an open shell state; doublet and triplet for $V_2Ti_2O_{10}^-$ and $VTi_3O_{10}^-$, respectively. For each additional titanium atom there is a $(-O)_3Ti-O\cdot$ unit with a free radical localized on a singly titanium-bonded terminal oxygen atom, O·. The length of the $Ti^{(-)}=O$ bond (163 pm) is comparable to the V=O bond (159 pm) and significantly shorter than the weaker Ti−O· bond (188 pm). Formation of two W−O· radical sites has also been shown for O-rich WO_n clusters [196].

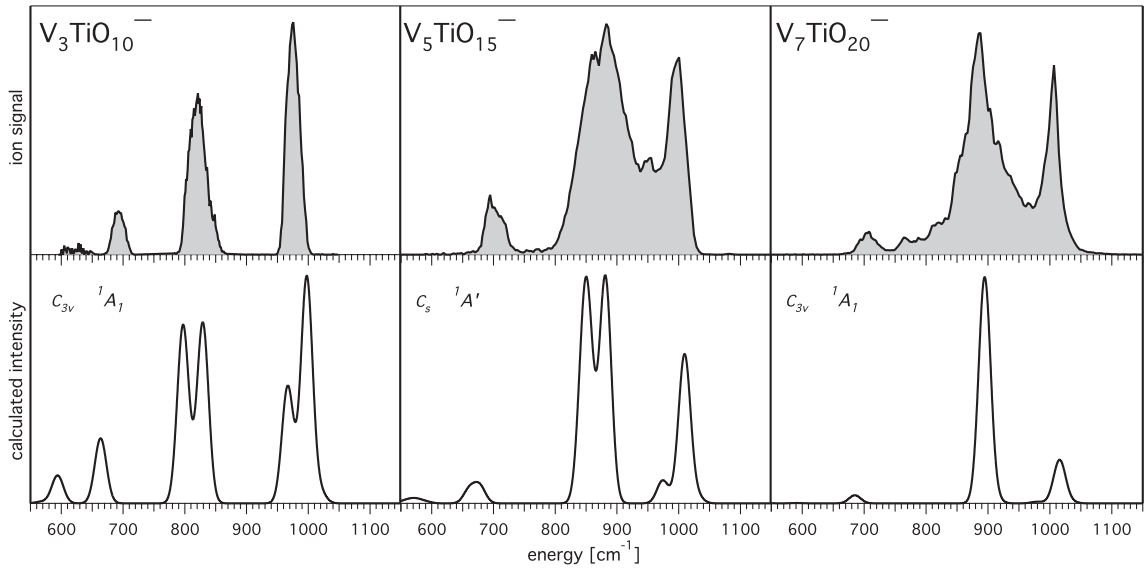

Figure 5.3: Experimental IR-PD spectra (top) and calculated IR spectra (bottom) of $V_3TiO_{10}^-$, $V_5TiO_{15}^-$, and $V_7TiO_{20}^-$ in the 550 to 1100 cm^{-1} range. The calculations are based on scaled harmonic frequencies of the B3LYP/TZVP optimized geometries.

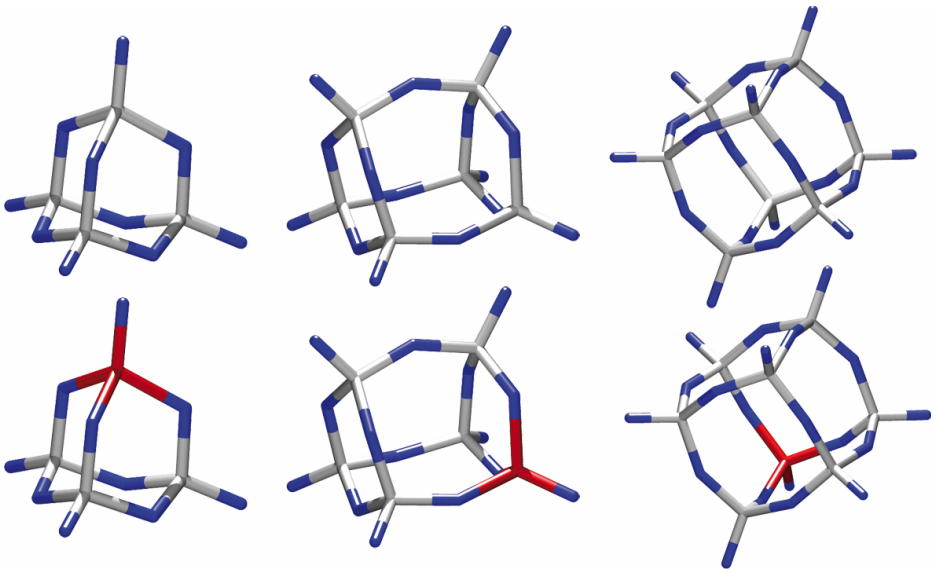

Figure 5.4: Structures for pure $(V_2O_5)_n^-$ (n=2–4) (top row) and $(V_2O_5)_{n-1}(VTiO_5)^-$ (n=2–4), i.e., single substitution of one vanadium atom by one titanium atom (bottom row). Vanadium atoms are depicted in light gray, titanium in red, and oxygen in blue.

Parent	Fragment(s)	Position of Observed Bands (cm^{-1})
$V_4O_{10}^-$	$V_3O_8^-$	990, 670(s), 637, 602
$V_3TiO_{10}^-$	$V_3O_8^-$	976, 821, 815(s), 810(s), 693, 628, 610
$V_2Ti_2O_{10}^-$	$VTi_2O_7^-$	979, 840(s), 816, 692, 679(s), 642, 619, 606
$VTi_3O_{10}^-$	$VTi_2O_7^-$	977, 669(s), 828, 791, 778, 751(s), 731, 725(s), 679, 651, 605
$Ti_4O_{10}^-$	$Ti_3O_7^-$	967, 963(s), 960(s), 885, 840(s), 828, 801(s), 718, 683, 666, 656, 641, 608, 597

Table 5.4: Experimental vibrational frequencies (in cm^{-1}) of the $V_{4-n}Ti_nO_{10}^-$ (n=0–4) cluster anions determined from the respective IR-PD spectra, measured monitoring fragment ion mass-selectively. Vibrational frequencies are determined from band maxima or estimated based on observable shoulders (s) formed by overlapping transitions.

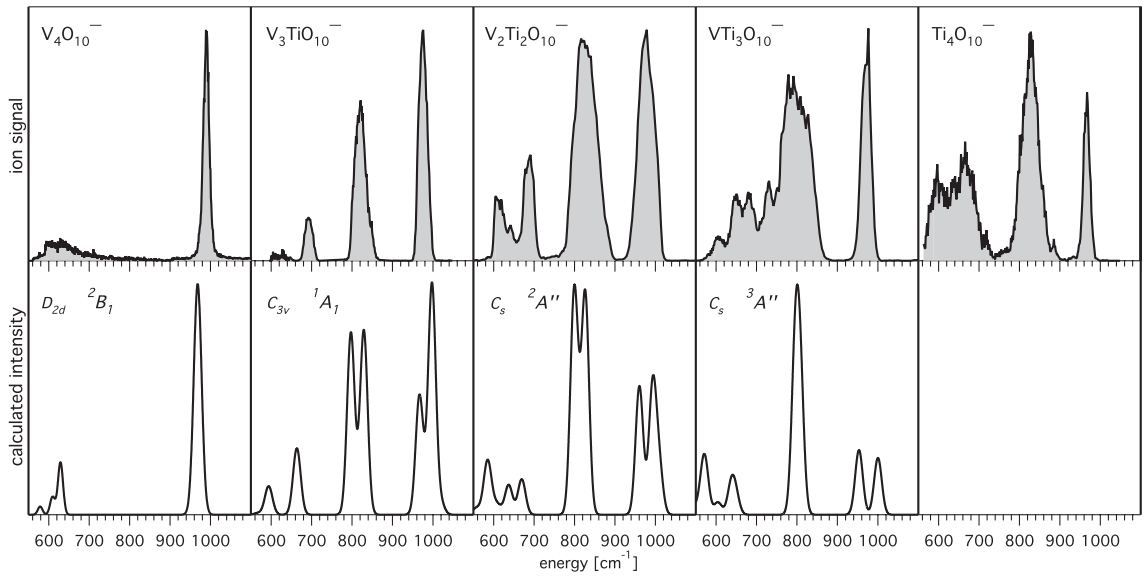

Figure 5.5: Experimental IR-PD spectra (top) for $V_{4-n}Ti_nO_{10}^-$ (n=0–4) in the 550 to 1100 cm^{-1} region, and calculated spectra (bottom) for n=0–3.

First DFT optimizations for $Ti_4O_{10}^-$ gave again a tetrahedral structure, similar to the one of all other clusters of the family. Recently, Sauer and coworkers found a

lower energy structure for $Ti_4O_{10}^-$ by employing a genetic algorithm to look for other possible isomers [197].

5.3.3 Comparison with Neutral Clusters

The singly substituted $(V_2O_5)_{n-1}(VTiO_5)^-$ (n=2–4) cluster anions are isoelectronic with neutral $(V_2O_5)_n$ clusters. Because neutral clusters are experimentally difficult to mass select it is of interest to check if one can characterize the structure of neutral clusters by performing experiments on the corresponding mixed, isoelectronic cluster anions. The calculated IR spectra and optimized structures for $(V_2O_5)_n$ (n=2–4) are shown in Figure 5.6. The calculated geometries are similar but of higher symmetry than the corresponding Ti-doped anions due to the presence of only one type of metal atoms. However, the measured IR spectra are indeed similar to those of the corresponding neutral counterparts.

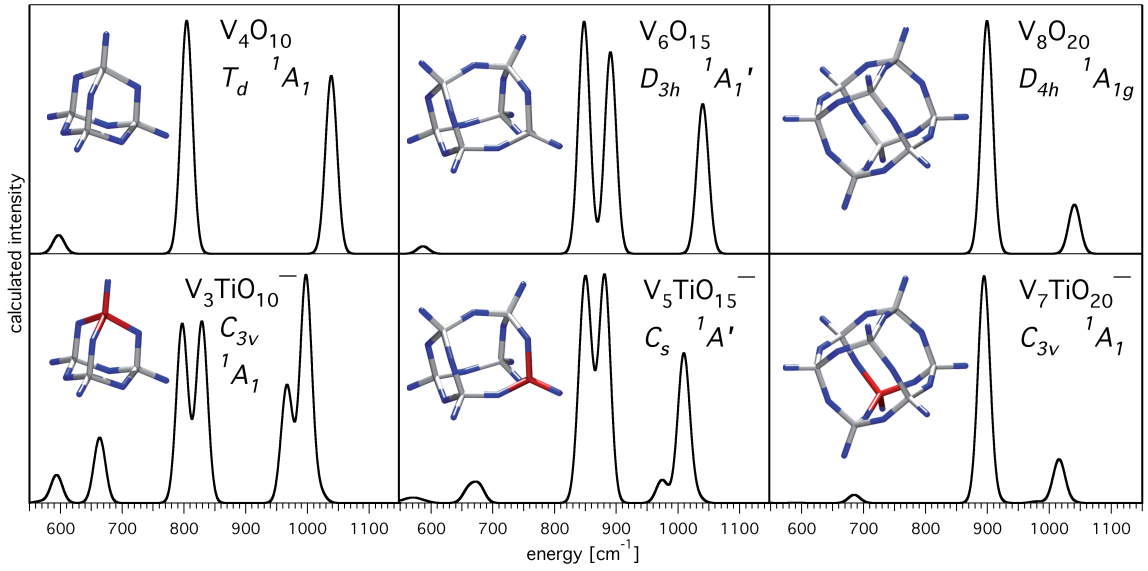

Figure 5.6: Calculated IR spectra and optimized structures for $(V_2O_5)_n$ (n=2–4) (top) and $(V_2O_5)_{n-1}(VTiO_5)^-$ (n=2–4) (bottom).

5.4 Summary

In this study, the first IR spectra for mixed metal oxides are measured. The doping of vanadium oxide cluster anions by titanium atoms is effectively employed to modify the electronic configuration of clusters without changing the overall geometric structures. The structures of the $(V_2O_5)_{n-1}(VTiO_5)^-$ (n=2–4) clusters are found to be the same

	$V_4O_{10}^-$	$V_3TiO_{10}^-$	$V_2Ti_2O_{10}^-$	$VTi_3O_{10}^-$
Ground state	$^2B_1$	$^1A_1$	^2A"	^3A"
# V=O	4	3	2	1
# $Ti^{(-)}$=O	0	1	1	1
# Ti−O·	0	0	1	2
# Unpaired e^-	1	0	1	2

Table 5.5: Electronic configurations of the $V_{4-n}Ti_nO_{10}^-$ (n=0–3) clusters.

as in the corresponding vanadium oxide cluster anions $(V_2O_5)_n^-$ (n=2–4) (except for the symmetry lowering due to the titanium atoms), while the number of electron is reduced by one, yielding closed-shell electronic structures. These doped clusters have the same electronic structure and the same geometry of the neutral counterpart.

Experimental characterization of the neutrals is often addressed by inference from information available only for the corresponding ions. But charge status and electronic structure can have a major effect on geometric structure (see Chapter 4). With the here presented atomic-substitution method, cluster ions are formed, which are isoelectronic to the neutrals keeping also the same geometry but differing in the chemical composition. This is, thus, a complementary approach to the indirect characterization of neutrals.

Also for the $V_{4-n}Ti_nO_{10}^-$ clusters the structures do not significantly change from n=0 to n=3, while different electronic structures are found. In particular, one unpaired electron is delocalized over the four vanadium atoms in the n=0 cluster; the n=1 cluster has no unpaired electrons; the n=2 (3) cluster is in a doublet (triplet) state with the unpaired electron(s) localized on one (two) terminal oxygen atom(s). These results are summarized in Table 5.5. It is therefore possible to modify not only the number of unpaired electrons but also their localization sites, while preserving the geometrical structure.

It has been shown with this study that the formation of mixed metal oxide cluster is feasible also controlling the relative quantities of the different metals. In a more general perspective, it will be interesting to apply this technique to the production of model systems to study the active site–support interaction. However, this study has also shown that the produced clusters are found in the global minimum structures, while this does not necessarily have to be the case for those clusters that model a metal oxide species deposited on a metal oxide support. Therefore, it is clear that this technique can be applied for the production of clusters that one wants to study in their ground state, but a different approach is necessary otherwise. One possible modification of the dual target source that may help in this direction, consists in separating the two metal targets, so that metal oxide clusters are formed independently and mixed when

they are already partially cooled down.